# Three-dimensional inversion of MT data based on equivalent transformation

Zhihao Rong[1], Yunhe Liu[1], Chuangchun Yin[1] and Libao Wang[2]
[1]College of Geo-Exploration Science and Technology, Jilin University, rongzh22@mails.jlu.edu.cn
[2]Shandong Huichuang Technology Co., Ltd

## SUMMARY

As a low-cost deep exploration technology, the magnetotelluric (MT) method has been widely used in the detection of deep electrical structures for studying geoscientific problems. With the expansion of the detection range and the requirement of high resolution, the conventional MT three-dimensional (3D) inversion methods face challenges. First, the electrically anisotropy caused by mantle inhomogeneity cannot be mimicked by isotropic models, and there don't exist mature methods for 3D MT anisotropic inversion. Second, the increase in research scale expands the spatial dimension of the inversion model, enhances the under-determination of inversion, and affects both convergence and stability. To solve these problems, we propose a 3D MT inversion method based on equivalent transformation. Through numerical experiments and measured data inversion, we prove that our new method can improve the stability and convergence efficiency of 3D MT anisotropic inversions.

**Keywords:** Magnetotelluric (MT), three-dimensional (3D), inversion, equivalent transformation, anisotropy.

## INTRODUCTION

MT signal is sensitive to underground conductive structures and its signals are not shielded by high-resistivity medium. Using natural-field as sources for exploration has lower costs and deeper exploration depths than other geophysical methods. This makes it widely used in the field of Deep Earth studies. The inhomogeneity of deep Earth media can easily generate the electrical anisotropy and affect MT data. Using the conventional methods to process these data often results in false structures (Rong et al., 2022). Therefore, the development of MT anisotropic forward modeling and inversion methods becomes a research hotspot.

Although two-dimensional (2D) methods can invert MT data fast, they are based on the assumption that MT data meets the 2D structure conditions via dimensional analysis and results have strong equivalence. With the improvement of computer hardware and numerical solution methods, 3D inversions have gradually become the mainstream research area. However, the anisotropic conductivity is a tensor (Yin, 2000; Yang and Lin, 2020), and its model dimension is 3~6 times that of isotropic model, which results in a strong under-determination and thus affects convergence. Blatter et al. (2021) used Gaussian processes to reduce the model order and improved the efficiency of 2D MT Bayesian inversion, Manassero et al. (2021) accelerated the 3D inversion of hexahedron grid through Kriging interpolation. All of them indicate that the model simplification is valuable for improving inversion efficiency. However, both of the above methods have hyperparameters (such as characteristic length scales), making them difficult to apply to 3D unstructured mesh. Madsen et al. (2020) used structured grids to construct a mapping between the unstructured inversion mesh and the forward mesh and achieved 3D time-domain inversions. The results showed that using a sparse mesh for inversion and a dense mesh for forward modeling can meet the resolution requirements. However, this method needs the pre-construction of a suitable structured grid, which is generally not easy to implement. Toth et al. (2017) pointed out that the number of elements in unstructured mesh is 4~6 times that of nodes. In this paper, we propose a 3D MT inversion method based on equivalent transformation, in which the forward modeling is executed by the finite-element (FE) method based on the dense unstructured mesh, while for the inversion the model space is transformed to the element nodes. A spatial mapping is constructed to achieve 3D MT inversions with model dimensionality reduction. We will prove via the numerical experiments of synthetic and field survey data inversions the convergence efficiency and stability of our method in comparison with the conventional methods.

## METHODS

### Forward Modeling

We use FE method to model the MT responses, the specific theory refers to Rong et al. (2022). Here we give a brief introduction. To obtain the electrical field, we solve the following curl-curl equation:

$$\nabla\times\nabla\times\boldsymbol{E}+\hat{i}\omega\mu_0\underline{\underline{\sigma}}\boldsymbol{E}=0\,. \tag{1}$$

where $\hat{i}$ is the imaginary unit, $\omega$ is the angular frequency, $\mu_0$ is the magnetic permeability in vacuum and $\underline{\underline{\sigma}}$ is the conductivity tensor ( refers to Yin, 2000). Using the vector basis function $\boldsymbol{N}$ as the weighting function, we obtain the governing equation in each element, i.e.

$$\begin{aligned}&\int_V(\nabla\times\boldsymbol{N}_i^e)\cdot(\nabla\times\boldsymbol{N}_j^e)dV\sum_{j=1}^{6}E_j^e\\&+\hat{i}\omega\mu_0\int_V\boldsymbol{N}_i^e\,\underline{\underline{\sigma}}\,\boldsymbol{N}_j^e\,dV\sum_{j=1}^{6}E_j^e=0\end{aligned}\,. \tag{2}$$

The integration in Eq. (2) can be found from Jin (2002). Assembling all equation (2) for all elements, we obtain the matrix equations, i.e.

$$\mathbf{KE}=\mathbf{b}\,. \tag{3}$$

After solving **E** for two polarizations, we can calculate the MT transfer function (TF), i.e.

$$\begin{bmatrix}Z_{xx}&Z_{xy}\\Z_{yx}&Z_{yy}\end{bmatrix}=\begin{bmatrix}E_x^1&E_x^2\\E_y^1&E_y^2\end{bmatrix}\cdot\begin{bmatrix}H_x^1&H_x^2\\H_y^1&H_y^2\end{bmatrix}^{-1}\,. \tag{4}$$

### Inversions

In order to transform the model space from unstructured mesh to element nodes, we define the following equivalent transformation for parameters:

$$\mathbf{F}\cdot\boldsymbol{\Theta}_k^*=\boldsymbol{\Theta}_k\,. \tag{5}$$

where **F** is the mapping matrix of the *m*×*n* dimension (*m* is the number of tetrahedrons, *n* is the number of nodes), and its elements are the volume coordinates of each tetrahedron. The superscript * refers to the parameter at the node, while the subscript *k* represents the $k^{\text{th}}$ anisotropic parameter. After Rong et al. (2023), the model parameters **m** is transformed to a new constraint domain $\boldsymbol{\Theta}$ for an implicit smooth model, i.e.

$$\boldsymbol{\Psi}=\mathbf{T}(\mathbf{m}), \tag{6}$$

$$\boldsymbol{\Theta}=\mathbf{C}_w(\boldsymbol{\Psi}-\boldsymbol{\Psi}^{pri})\,. \tag{7}$$

Eq. (6) is a logarithmic transformation to constrain the value of the parameter.

Now, we can construct a regularized objective function in sparse model space, i.e.

$$\Phi^*=\Phi_d+\lambda\Phi_c^*\,, \tag{8}$$

where $\lambda$ is a regularization factor to prevent false structures caused by overfitting. We use $L_2$-norm to construct the data-fitting term $\Phi_d$ and calculate it in dense model space. But for the model constraint $\Phi_c^*=\sum\left\|\Theta_k^*\right\|_2^2$, we calculate it in sparse model space. According to the chain rule, the gradient of the objective function with respect to model parameters can be calculated by

$$\mathbf{g}_k=-2\mathbf{F}^T(\mathbf{C}_w^{-1})^T\mathbf{C}_p^T\mathbf{J}_k^T\mathbf{v}+2\lambda\boldsymbol{\Theta}_k^*\,. \tag{9}$$

where **J** is the sensitivity in dense model space and is calculated by the adjoint forward modeling. After obtaining the gradient, the limited-memory quasi-newton method (refers to Liu and Nocedal, 1989) is used to optimize Eq. (8) until the data fitting converges to a certain level to obtain the optimal anisotropic model.

### Matrix Analysis

As Eq. (5) and (7) can automatically and iteratively update, the matrix $\mathbf{C_w}$ and $\mathbf{F}^{-1}$ do not need to be calculated. But as $\mathbf{C_w}^{-1}$ is a full-rank square matrix, its inverse can easily be calculated by solving an adjoint problem, i.e.

$$\underbrace{\mathbf{C}_w^{-1}}_{\mathbf{A}}\underbrace{[\mathbf{C}_w(\boldsymbol{\Psi}^n-\boldsymbol{\Psi}^{pre})]}_{\mathbf{x}}=\underbrace{(\boldsymbol{\Psi}^n-\boldsymbol{\Psi}^{pre})}_{\mathbf{b}}\,. \tag{11}$$

Unfortunately, **F** is not a square matrix, its inverse can only be obtained by using mathematical techniques such as singular value decomposition to obtain a pseudo inversion. The inverse calculation is time-consuming and complex, so we define the following spatial mapping operator to describe the relationship between the two spaces (Dense Space and Sparse Space):

$$\begin{cases}\mathbf{F}_1\cdot\mathbf{DS}=\mathbf{SS}\\\mathbf{F}_2\cdot\boldsymbol{\delta}_{\mathbf{SS}}=\boldsymbol{\delta}_{\mathbf{DS}}\end{cases}\,. \tag{12}$$

where $\mathbf{F}_2=\mathbf{F}$, but $\mathbf{F}_1$ is a new matrix whose elements are the volume weight of tetrahedra that share the same nodes.

## RESULTS

### Numerical Experiments

To verify the effectiveness of our method, we first design a chessboard model with 9 chess pieces and principal-axis anisotropy, which were divided into groups based on the principal axis conductivity (rho-x/rho-y/rho-z = 10/1000/100 ohm-m) and (rho-x/rho-y/rho-z = 1000/10/100 ohm-m). All pieces with 25 km of top depth. After obtaining the impedance data for 289 MT sites via forward modeling, we add 3% Gaussian random noise to them for our inversion, with a total of 12 logarithmically equidistant frequencies from 0.0001 to 0.1 Hz. To obtain accurate EM responses, we divide the forward model into 706060 tetrahedra, while for the inverse model, the finely-discretized abnormal bodies are removed, resulting in 594383

tetrahedra. Our new method uses tetrahedral nodes as a sparse model for a total of 101660 points (which reduces the number of elements by nearly 6 times).

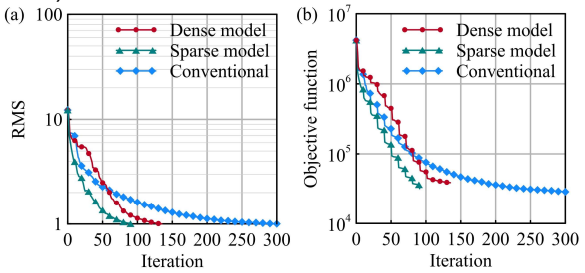


**Figure 1.** Comparison of the convergence using the different inversion methods. RMS is defined as the normalized root mean square of the data fitting. The blue lines indicate the iteration parameters of conventional constraint method's, the red ones are for the gradient filtering regularization method, while the green ones are from our method.

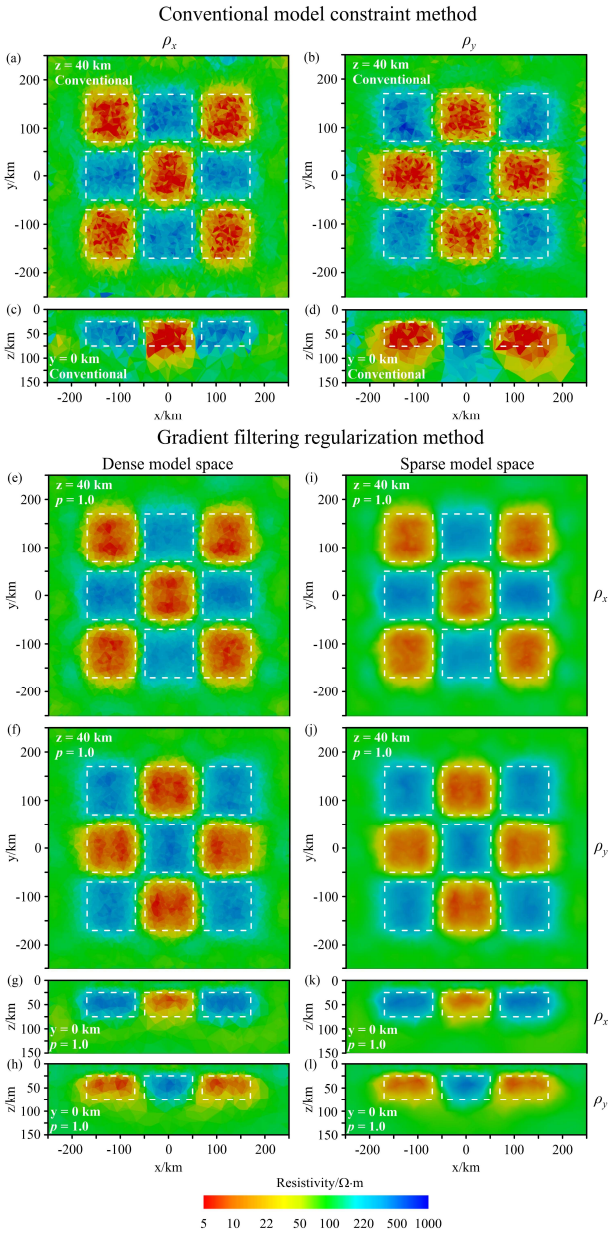


**Figure 2.** Comparison of the inversion results using different methods. (a)~(d) are slices for the conventional constraint method, (e)~(h) are for the gradient filtering regularization method with the dense model space, while (i)~(l) are for our new method. The white boxes indicate the boundary of the real anomaly body.

We use respectively the conventional model constraint (Liu et al., 2019; Rong et al., 2022), the gradient filtering regularization (Rong et al., 2023), and our new method to invert the data under the same initial model (a homogeneous half-space of 100 ohm-m) and inversion parameters. All methods converge to the same level.

Figure 1 shows the convergence of different inversion methods, while Figure 2 shows the slices of their inversion results at z=40km. It is easy to see that our new method converges the fastest and the results are closest to the true values, and clear boundaries of anomalous bodies and the smoothest imaging can be seen.

## Field Data Inversion

The data in this study were obtained from 298 long-period MT stations from the AusLAMP array (see Figure 3). These stations are spaced approximately 0.5° apart (~55 km), covering an area of 950 × 950 km. The details regarding the data acquisition and processing can be found in Kirkby et al. (2020). The original data have varying periods, ranging from 6.4s to 40,000s. We have selected 17 periods within this range, spanning from 15.8 s to 25,200 s. The size of the whole inversion model including the expansion area is 10000 × 10000 × 10000 km (including 5000 km of air layer). The model is discretized into 693181 tetrahedral elements. The shape of the ocean in the model is determined by the coastline of Southeast Australia.

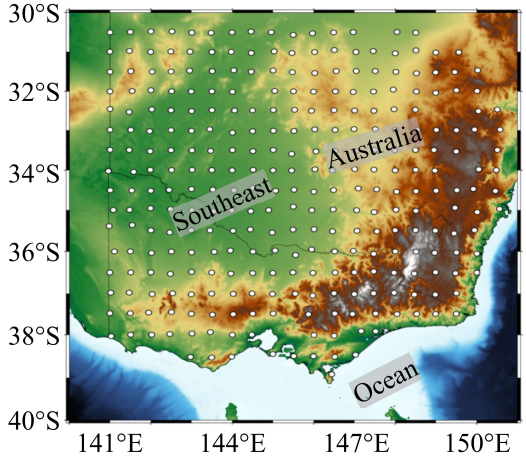


**Figure 3.** Distribution of MT survey sites in Southeast Australia. The white dots mark survey stations.

After analyzing these data, we find that they contain anisotropic characteristics. Therefore, we conducted anisotropic inversion to these data using different methods and comparing the results with those from an isotropic inversion based on an equivalent transformation. Similar to the conclusion of previous numerical experiments, the convergence, stability, and results of our new method are all the best among these methods. We cannot present them here for the page limitation and we will present them at the workshop.

## Conclusions

We have developed a 3D MT inversion method based on equivalent transformation and conducted experiments using a principal-axis anisotropic model. The results showed that our method has better convergence and stability than the conventional methods. It reduces the under-determination of 3D inversion to a certain extent and thus is suitable for efficient solutions of 3D inversion problems based on unstructured mesh. We also applied the method to AusLAMP field data inversion and recovered the anisotropic electrical structure under Australia that will be presented at the workshop.

## Acknowledgements

We thank the AuScope and AusLAMP projects for providing free field data for academic research. The geological figure here was plotted by Generic Mapping Tools (Wessel et al., 2013). The work was financially supported by the National Natural Science Foundation of China (42030806, 423B2405, 42074120, 42274093, 42174167, and 42004125).

## References

Blatter D, Ray A, Key K (2021) Two-dimensional Bayesian inversion of magnetotelluric data using trans-dimensional Gaussian processes. Geophysical Journal International 226(1): 548-563.

Jin JM (2002) The finite element method in electro--magnetics. Wiley-IEEE Press, New York.

Kirkby AL, Musgrave RJ, Czarnota K, Doublier MP, Duan J, Cayley RA, Kyi D (2020) Lithospheric architecture of a Phanerozoic orogeny form magnetotelluric: AusLAMP in the Tasmanides, southeast Australia. Tectonophysics 793: 228560. doi:10.1016/j.tecto.2022.228560

Liu DC, Nocedal J (1989) On the limited memory BFGS method for large scale optimization. Math Program 45: 503-528.

Liu YH, Yin CC, Qiu CK, Hui ZJ, Zhang B, Ren XY, Weng AH (2019) 3-D inversion of transient EM data with topography using unstructured tetrahedral grids. Geophysical Journal International 217: 301-318.

Madsen LM, Fiandaca G., Auken E. (2020) 3-D time domain spectral inversion of resistivity and full-decay induced polarization data; full solution of Poisson's equation and modelling of the current waveform. Geophysical Journal International 223(3): 2101-2116.

Manassero MC, Afonso JC, Zyserman FI, Jones AG, Zlotnik S, Fomin I (2021) A reduced order approach for probabilistic inversions of 3D magnetotelluric data II: Joint inversion of MT and surface-wave data. Journal of Geophysical Research: Solid Earth 126: e2021JB021962. doi:10.1029/2021JB021962

Rong ZH, Liu YH, Yin CC, Wang LY, Ma XP, Qiu CK, Zhang B, Ren XY, Su Y, Weng AH (2022) Three-dimensional magnetotelluric inversion for arbitrarily anisotropic earth using unstructured tetrahedral discretization. Journal of Geophysical Research: Solid Earth 127: e2021JB023778. doi:10.1029/2021JB023778

Rong ZH, Liu YH, Yin CC, Ma XP, Wang LY, Qiu CK, Zhang B, Ren XY, Su Y (2023) Gradient filtering regularization for 3-D MT inversion based on unstructured tetrahedral discretization. Geophysical Journal International 235(1): 94-108.

Toth CD, O'Rourke J, Goodman JE (2017) Handbook of Discrete and Computational Geometry (3rd ed.). Chapman and Hall/CRC Press.

Wessel P, Smith WH, Scharroo R, Lius J, Wobbe F (2013). Generic mapping tools: improved version released. Eos 94(95): 409-410.

Yang CF, Qin LJ (2020) Graphical representation and explanation of the conductivity tensor of anisotropic media 41: 249-281. doi:10.1007/s10712-019-09581-5

Yin CC (2000) Geoelectrical inversion for a one-dimensional anisotropic model and inherent non-uniqueness. Geophysical Journal International 140(1): 11-23.